Exploring the mechanism of action of glaucocalyxin D against acute myeloid leukemia using network pharmacology, molecular docking and cellular experiments

LIAN CHEN[1-3], WEIXIAN YANG[1,2], WEIQING ZHANG[2], HENG LUO[3] and CHEN YAN[1,2]

[1]College of Pharmaceutical Science, Guizhou University of Traditional Chinese Medicine, Guiyang, Guizhou 550025, P.R. China; [2]Department of Pharmacy, Anshun City People's Hospital, Anshun, Guizhou 561000, P.R. China; [3]State Key Laboratory of Discovery and Utilization of Functional Components in Traditional Chinese Medicine, Natural Products Research Center of Guizhou Province, Guizhou Medical University, Guiyang, Guizhou 550014, P.R. China

Received November 12, 2025; Accepted March 18, 2026

DOI: 10.3892/ol.2026.15622

Abstract. Glaucocalyxin D (GLD), an ent-kaurane diterpenoid isolated from *Isodon* species, exhibits extensive pharmacological potential; however, its mechanism of action against acute myeloid leukemia (AML) remains to be elucidated. The present study employed a combined network pharmacology and experimental approach to elucidate the anti-AML mechanisms of GLD. Potential targets were identified using database mining and a protein-protein interaction network was constructed. The Gene Ontology and the Kyoto Encyclopedia of Genes and Genomes enrichment analyses highlighted the JAK-STAT signaling pathway as central to action by GLD. Molecular docking predicted stable binding of GLD to core targets, including STAT3. Experimental validation in HEL and K562 AML cells demonstrated that GLD potently and dose-dependently inhibits cell proliferation, with efficacy similar to the standard chemotherapeutic agent doxorubicin. Mechanistically, GLD suppressed the phosphorylation of JAK2 and STAT3. GLD also induced mitochondrial apoptosis by modulating the Bcl-2/Bax ratio and triggered G_2/M phase arrest by downregulating cyclin B1 and CDK1. These findings delineated a coherent mechanism whereby GLD exerts anti-leukemic effects by inhibiting the JAK-STAT pathway, supporting its potential as a novel lead compound for AML therapy in the future.

Correspondence to: Dr. Chen Yan, Department of Pharmacy, Anshun City People's Hospital, 140 Huangguoshu Road, Anshun, Guizhou 561000, P.R. China
E-mail: nazi3647@sina.com

Professor Heng Luo, State Key Laboratory of Discovery and Utilization of Functional Components in Traditional Chinese Medicine, Natural Products Research Center of Guizhou Province, Guizhou Medical University, 3491 Baijin Avenue, Shawen Ecological Science and Technology Industrial Park, Guiyang National High-Tech Industrial Development Zone, Guiyang, Guizhou 550014, P.R. China
E-mail: luoheng71050@aliyun.com

Key words: glaucocalyxin D, acute myeloid leukemia, network pharmacology, molecular docking, JAK-STAT signaling pathway

Introduction

Acute myeloid leukemia (AML) is a common hematological malignancy caused by the clonal expansion of undifferentiated myeloid progenitors (1,2). Globally, AML accounts for ~1.5% of all new cases of cancer and remains one of the most lethal hematological malignancies, with a 5-year survival rate of <30%, The resulting hematopoietic failure represents a primary cause of patient mortality (3). Although chemotherapy, radiotherapy and hematopoietic stem cell transplantation are the current mainstays of treatment, the frequent development of multidrug resistance leads to limited efficacy and poor prognosis (4). Therefore, the identification of novel, naturally derived active compounds with distinct mechanisms of action, low toxicity and high efficacy remains a key direction in AML drug development.

Natural products and their derivatives have been a vital source of antitumor agents (5,6). Diterpenoids derived from plants of the genus *Isodon suzhouens* have gained increasing attention due to their notable antitumor activities (7-9). Family members such as glaucocalyxin A (GLA) and B have been confirmed to induce apoptosis and autophagy in various tumor models by modulating pathways including PI3K/AKT. There are preliminary reports on the pro-apoptotic mechanisms of GLA in AML (10-13). However, the pharmacological mechanism of action of its structural congener, glaucocalyxin D (GLD), which demonstrates potent *in vitro* activity against chronic myeloid leukemia K562 cells (IC_{50}=1.60 μmol) (14), remains largely unexplored in the context of AML. Specifically, whether GLD exerts its effects through unique targets and signaling pathways is unknown and the characteristics of the types of cell death and cell cycle arrest GLD induces require systematic elucidation. This lack of mechanistic insight severely hinders the evaluation of its clinical translation potential.

Network pharmacology provides a powerful methodological framework in elucidating the complex interactions between compounds and diseases at a systems level by integrating systems biology and network analysis to establish multi-level associations among compounds, targets and disease states (15,16). The present study aimed to systematically investigate the anti-AML activity of GLD and elucidate its underlying molecular mechanisms through an integrated approach combining network pharmacology, molecular docking and *in vitro* experimental validation.

Materials and methods

Cell lines and reagents. HEL and K562 cell lines were provided by the State Key Laboratory of Discovery and Utilization of Functional Components in Traditional Chinese Medicine, Natural Products Research Center of Guizhou Province. RPMI-1640 culture medium was purchased from Gibco (cat. no. 11875093; Thermo Fisher Scientific, Inc.) and fetal bovine serum was supplied by Biological Industries (cat. no. 04-007-1A; Sartorius AG). Furthermore, penicillin-streptomycin solution (100X), MTT reagent and phosphate-buffered saline (PBS) were acquired from Beijing Solarbio Science & Technology Co., Ltd. (cat. nos. P1400; IM0280; P1020). The present study also used the Annexin V-FITC/PI apoptosis detection kit (cat. no. C1383M; Beyotime Biotechnology) and the cell cycle analysis kit (cat. no. C1052; Beyotime Biotechnology).

Isolation and characterization of GLD. GLD was isolated from Isodon suzhouensis aerial parts. Dried material ($1.00x10^8$ mg) was extracted with 95% ethanol and partitioned between water and ethyl acetate to yield the ethyl acetate fraction ($3.60x10^6$ mg). This fraction was subjected to silica gel column chromatography (300-400 mesh; Qingdao Haiyang Chemical Co., Ltd., Qingdao, China) using stepwise gradient elution with petroleum ether-acetone (80:1→1:1, v/v). Fraction 5 was further separated on silica gel with petroleum ether-acetone (15:1→1:1, v/v). Subfraction Fr.5.2 was purified by D-101 macroporous resin (Cangzhou Bon Adsorber Technology Co., Ltd., Cangzhou, China) with ethanol-water (30→70%, v/v) to yield GLD (40 mg) (14). Purity (>98%) was determined by analytical HPLC using a Waters 1525 EF system (Waters Corporation, Milford, MA, USA) on a YMC C18 column (4.6x250 mm, 5 μm; YMC Co., Ltd., Kyoto, Japan) at 30˚C. The mobile phase consisted of water and methanol (55:45, isocratic; no gradient was used) at a flow rate of 1.0 ml/min. The injection volume was 10 μl, and detection was performed at 239 nm using a ZF-1 UV analyzer (Shanghai Baoshan Guncun Electro-optical Instrument Factory, Shanghai, China) (Fig. S1). No internal standard was used. The structure was confirmed by NMR and MS. NMR spectra were recorded on a Varian INOVA 600 MHz spectrometer (Varian, Inc., Palo Alto, CA, USA) at 600 MHz for ^{1}H and 150 MHz for ^{13}C in $CDCl_3$ with tetramethylsilane (TMS) as the internal standard. HR-MS was performed on a Waters Autospec Premier P776 mass spectrometer (Waters Corporation, Milford, MA, USA). The NMR and MS data were consistent with the literature (Figs. S2 and S3).

Cell culture. HEL and K562 cells were cultured in RPMI-1640 medium supplemented with 10% fetal bovine serum and 1% penicillin-streptomycin at 37˚C in a humidified atmosphere with 5% CO_2.

Network pharmacology analysis. Obtaining the intersection genes of GLD and AML potential molecular targets of GLD were identified by screening the PharmMapper (http://lilab.ecust.edu.cn/pharmmapper/) and SwissTargetPrediction (http://www.swisstargetprediction.ch/) databases. Targets associated with AML were retrieved by querying the GeneCards (https://www.genecards.org/), Online Mendelian Inheritance in Man (OMIM) (http://www.omim.org) and Therapeutic Target Database (TTD) (https://db.idrblab.net/ttd) using the key word 'acute myeloid leukemia'. Standardized gene nomenclature was ensured by referencing the UniProt database (https://www.uniprot.org/). Subsequently, overlapping genes between GLD targets and AML-associated genes were determined using Venny 2.1.0 (Spanish National Biotechnology Centre, Madrid, Spain; https://bioinfogp.cnb.csic.es/tools/venny/).

Construction of protein interaction networks and core target screening. The identified drug-disease intersection targets were input into the Search Tool for the Retrieval of Interacting Genes/Proteins (STRING) database (https://string-db.org/), with the target species set to *Homo sapiens* and a minimum interaction score threshold of 0.4. Peripheral-free targets were excluded to generate a network interaction diagram and a tab-separated values (TSV) file illustrating target interactions. This TSV file was then imported into Cytoscape (version 0.1. https://apps.cytoscape.org/apps/cytohubba) to construct the protein-protein interaction (PPI) network diagram. The 'cytoHubba' and 'molecular complex detection MCODE (version 1.2; https://apps.cytoscape.org/apps/mcode) plugins were used for network topology analysis, producing the most significant core target network diagram and the clustered network relationship diagram, respectively.

GO and KEGG analyses. The intersecting genes were imported into the Database for Annotation, Visualization and Integrated Discovery (DAVID) database (version 6.8; https://david.ncifcrf.gov/). The present study selected *Homo sapiens* for Gene Ontology (GO) functional enrichment analysis and Kyoto Encyclopedia of Genes and Genomes (KEGG) pathway enrichment analysis to identify key signaling pathways. Data analysis and visualization were conducted using the MicroBioinformatics online platform (version 1.0; Shanghai BioGenius Biotechnology Co., Ltd.).

Molecular docking. The top 10 core targets of GLD, ranked by their binding affinity, were subjected to molecular docking analysis. The three-dimensional structures of the target proteins were retrieved from the Protein Data Bank (PDB) database (https://www.rcsb.org/). The target proteins were processed by removing ligands and water molecules, followed by hydrogenation using 'AutoDockTools' (version 1.5.6; Molecular Graphics Laboratory; Scripps Research Institute). Both the protein receptors and ligands were then converted into PDB, partial charge and atom type format. Molecular

docking was performed using AutoDock Vina (version 1.2.0; Molecular Graphics Laboratory; Scripps Research Institute) software and the model with the lowest free energy was selected for analysis. The results were visualized using PyMOL (version 2.5; Schrödinger, Inc.) software. Each interaction was assigned a docking score, with lower scores indicating improved docking quality.

Cell viability assay. The MTT method was used to evaluate cell viability. Briefly, cells were seeded into 96-well plates at a density of $5x10^3$ cells per well. After 24 h, the cells were treated with different concentrations of GLD (0.625, 1.25, 2.5, 5 and 10 μmol/l) dissolved in DMSO (0.1% v/v) for 24, 48 and 72 h, and doxorubicin was used as a positive control. Following treatment, MTT reagent was added for 4 h, the formazan crystals were dissolved in DMSO (≥99.9%), and absorbance was measured at 490 nm using an ELx808 microplate reader (Agilent Technologies, Inc) Cell viability was calculated relative to untreated controls.

Detection of apoptosis by Hoechst 33258 staining. To detect cell apoptosis, the cells were seeded into 6-well plates at a density of $3x10^5$ cells per well. After treatment with GLD for 48 h, cells were collected, washed with PBS and fixed with 4% paraformaldehyde at room temperature for 15 min. Following fixation, cells were washed twice with PBS and stained with Hoechst 33258 (5 μg/ml, 0.5% v/v) for 10 min at room temperature in the dark. After washing to remove excess stain, cells were resuspended in a small volume of PBS. A drop of the cell suspension was mounted with anti-fade mounting medium, covered with a coverslip and immediately observed under a fluorescence microscope. Apoptotic cells were identified by the presence of condensed and fragmented nuclei.

Apoptosis detection and cell cycle analysis. For the detection of apoptosis and cell cycle analysis, cells were seeded in 6-well plates at a density of $3x10^5$ cells per well. Using DMSO (0.1% v/v) as the control group, cells were treated with different concentrations of GLD for 48 h. Subsequently, cells were collected and stained using the Annexin V-FITC/PI apoptosis detection kit (cat. no. C1062M; Beyotime Biotechnology) and the cell cycle analysis kit (cat. no. C1052M; Beyotime Biotechnology) for flow cytometry (BD Biosciences). Staining was performed at room temperature for 15 min in the dark, according to the manufacturer's instructions. No intracellular cytokine staining was performed. The collected data were analyzed using FlowJo software (version 10.10; BD Biosciences). For apoptosis analysis, cells were gated on forward scatter/side scatter to exclude debris and the percentage of Annexin V-FITC-positive and PI-positive cells was determined. For cell cycle analysis, single cells were gated, and the proportions of cells in G_1, S and G_2M phases were calculated using the Dean-Jett-Fox model (17).

Western blotting. After treatment with GLD for 48 h, cells were harvested and washed with PBS. Total proteins were extracted using radioimmunoprecipitation assay lysis buffer (cat. no. P0013B; Beyotime Biotechnology; RIPA:PMSF=100:1)) supplemented with a protease inhibitor cocktail (cat. no. P1005; Beyotime Biotechnology). Cell lysis was performed on ice, followed by brief sonication (20 kHz; 4˚C; 10 sec on, 10 sec off for 2 cycles). The lysates were centrifuged at 12,000 x g for 15 min at 4˚C to collect the supernatant. Protein concentration was determined using the BCA Protein Assay Kit (cat. no. P0012; Beyotime Biotechnology) according to the manufacturer's instructions. Equal amounts of protein (30 μg per lane) were mixed with 5X loading buffer, denatured at 95˚C for 10 min and separated by 10% sodium dodecyl sulfate-polyacrylamide gel electrophoresis. The separated proteins were then transferred onto polyvinylidene fluoride membranes. The membranes were blocked with 5% bovine serum albumin in Tris-buffered saline with 0.1% Tween 20 for 2 h at room temperature and subsequently incubated overnight at 4˚C with the following primary antibodies (all diluted 1:1,000): Anti-phosphorylated (p)-JAK2 (Tyr1007/1008; cat. no. 3771; Cell Signaling Technology, Inc.), anti-JAK2 (cat. no. 17670-1-AP; Proteintech Group Inc.), anti-p-STAT3 (Tyr705; cat. no. 9145; Cell Signaling Technology, Inc.), anti-STAT3 (cat. no. 10253-2-AP; Proteintech Group Inc.), anti-Bcl-2 (cat. no. 12789-1-AP; Proteintech Group Inc.), anti-Bax (cat. no. 50599-2-Ig; Proteintech Group Inc.), anti-cyclin B1 (cat. no. 55004-1-AP; Proteintech Group Inc.), anti-p-CDK1 (Tyr15; cat. no. 4539; Cell Signaling Technology, Inc.) and anti-β-actin (anti-β-actin (cat. no. 66009-1-Ig; Proteintech Group Inc.) and anti-GAPDH (cat. no. 60004-1-Ig; Proteintech Group Inc.). After washing, the membranes were incubated with horseradish peroxidase-conjugated goat anti-rabbit IgG secondary antibody (1:50,000; cat. no. SA00001-2; Proteintech Group Inc.) for 2 h at room temperature. Protein bands were visualized using an enhanced chemiluminescence (ECL) detection kit (cat. no. P0018FS; Beyotime Biotechnology) and the band intensities were semi-quantified using ImageJ software (version 1.54; National Institutes of Health). The expression levels of target proteins were normalized to β-actin or GAPDH.

Statistical analysis. Statistical analyses were performed using GraphPad Prism software (version 9.5.1; Dotmatics). Data from at least three independent experiments are presented as mean ± standard deviation. Comparisons among multiple groups were conducted using one-way analysis of variance, followed by Tukey's honest significant difference post hoc test for multiple comparisons. $P<0.05$ was considered to indicate a statistically significant difference.

Results

Network pharmacology. Active components and potential targets of GLD in AML were investigated in the present study. In total, 74 potential targets associated with GLD were retrieved from the PharmMapper and SwissTarget prediction databases. Concurrently, 5,576 targets were identified using the term AML in the OMIM, GeneCards and TTD databases (Fig. 1A). The Venny 2.1.0 online tool (https://bioinfogp.cnb.csic.es/tools/venny/) was used to identify the 55 overlapping targets between the 74 GLD-associated targets and the 5,576 AML-associated targets (Fig. 1B).

Construction of the PPI interaction network and identification of core targets. The 55 intersecting genes were input into the STRING database and a PPI network was constructed

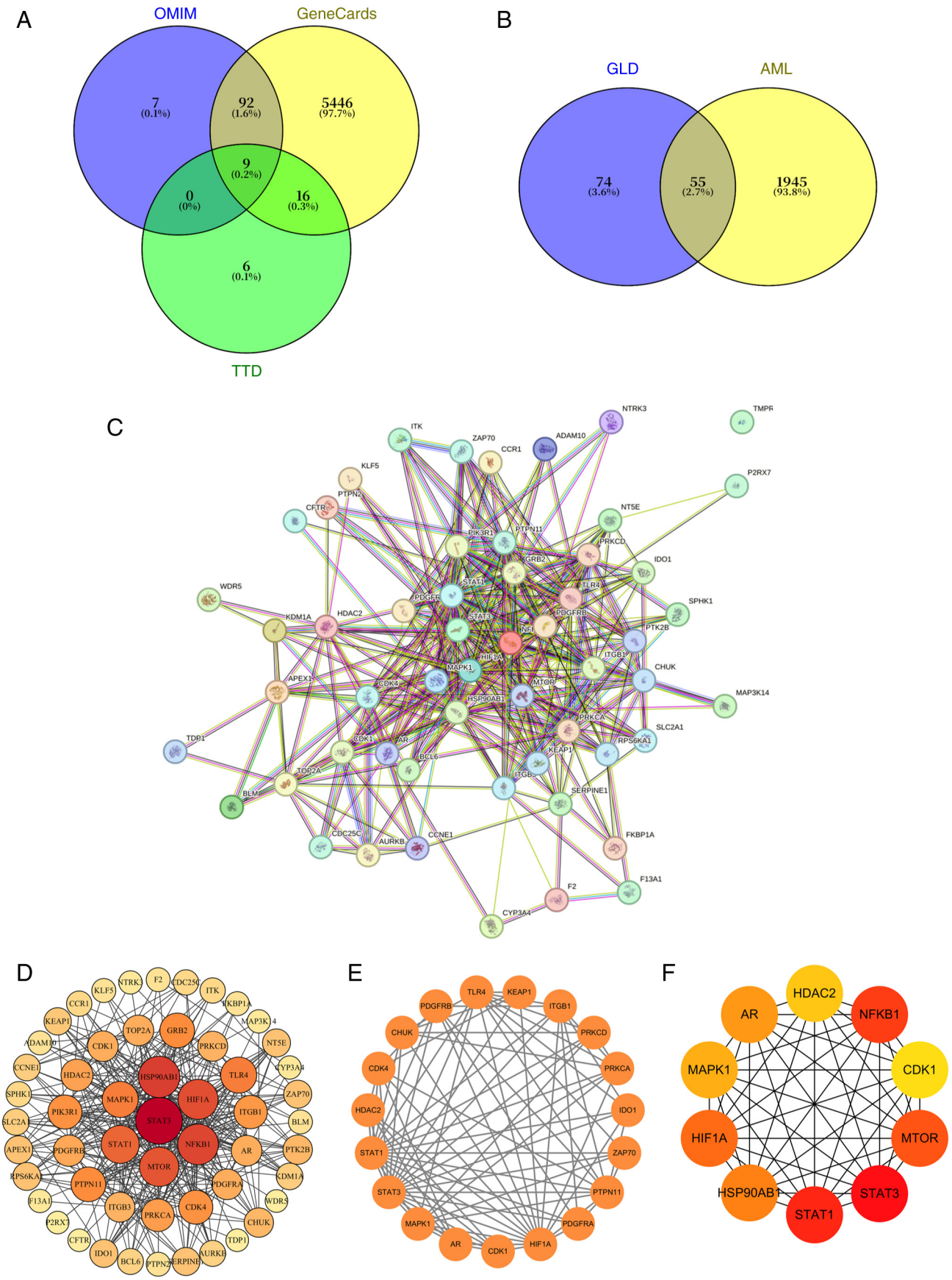

Figure 1. Potential AML-associated targets of GLD. (A) Venn diagram of AML-associated target interactions. The numbers of targets retrieved from the OMIM, GeneCards and TTD databases are shown: OMIM, 92; GeneCards, 5,446; TTD, 16. (B) Venn diagram of GLD and AML target intersections. A total of 74 GLD-associated targets and 5,576 AML-associated targets were analyzed, yielding 55 overlapping targets. (C) Construction of the GLD and AML gene-protein interaction network. The network was generated using the STRING database and visualized in Cytoscape. (D) Screening of core targets for GLD treatment of AML using the cytoHubba plugin. (E) Screening of core targets using the MCODE plugin. (F) Combined core target network diagram. AML, acute myeloid leukemia; GLD, glaucocalyxin D; OMIM, Online Mendelian Inheritance in Man; TTD, Therapeutic Target Database.

using the Cytoscape software (Fig. 1C). Subsequently, the core regions of the network were analyzed using 'cytoHubba' and 'MCODE' plugins, ultimately yielding three core topological networks (Fig. 1D-F). These networks encompassed 10 key targets: STAT3, nuclear factor-κ B subunit 1 (NFKB1), heat shock protein 90 kDa α, class B, member 1 (HSP90AB1), hypoxia-inducible factor-1α (HIF1A), mTOR, STAT1, MAPK1, toll-like receptor 4 (TLR4), growth factor receptor-bound protein 2 (GRB2) and protein tyrosine phosphatase non-receptor type 11 (PTPN11).

GO and KEGG enrichment analyses reveal the potential multi-target mechanism of GLD in AML. To elucidate the biological functions and pathways associated with the 55 overlapping targets, GO and KEGG enrichment analyses were performed. The GO analysis indicated that these targets are significantly involved in key oncogenic processes, including the 'positive regulation of phosphatidylinositol 3-kinase/protein kinase B signal transduction', 'positive regulation of cell migration' and 'positive regulation of angiogenesis' (biological process). They are primarily located in the 'nucleoplasm' and 'cytoplasm' (cellular component) and possess molecular functions such as 'protein kinase binding' and 'histone H3Y41 kinase activity' (molecular function) (Fig. 2A). These enriched terms collectively suggested that GLD may interfere with AML progression by broadly impacting signal transduction, cell motility and epigenetic regulation. KEGG pathway enrichment analysis of the predicted targets revealed 20 key signaling pathways potentially modulated by GLD (Table I). Pathways closely associated with cancer and immunoinflammatory responses, such as 'proteoglycans in cancer', 'JAK-STAT signaling pathway' and 'chemical carcinogenesis-receptor activation' were among the most significantly enriched. Notably, 9.5 targets were specifically enriched in the 'JAK-STAT signaling pathway', strongly suggesting its central role in the anti-AML activity of GLD (Fig. 2B). Subsequent molecular docking analysis demonstrated that GLD could form stable binding conformations with core proteins JAK2/STAT3 pathway, including JAK2 and STAT3, providing direct computational evidence for further experimental validation.

Molecular docking validates the direct binding of GLD to key signaling targets. To structurally validate the predictions from network pharmacology, molecular docking was performed to assess the binding of GLD to core targets. The results demonstrated strong binding affinities (ΔG <-5.0 kcal/mol) between GLD and several pivotal targets (Table II). Of note, GLD exhibited high affinity for STAT3 (ΔG=-6.3 kcal/mol), the central transcription factor within the significantly enriched 'JAK-STAT signaling pathway', corroborating the KEGG enrichment analysis. Docking poses suggested that GLD binds to the Src homology 2 domain of STAT3, a key site for phosphotyrosine binding and dimerization, implying a potential mechanism for direct interference with its activation. Notable binding was also observed for other relevant targets, including MAPK1 (-6.8 kcal/mol) and STAT1 (-6.6 kcal/mol). Visualization of the optimal binding conformations (Fig. 3A-J) revealed stabilizing interactions mediated by hydrogen bonds and hydrophobic forces. These findings provided notable computational structural evidence that GLD can directly engage with key effectors like STAT3 and potentially modulate the associated signaling networks.

GLD inhibits the proliferation of AML cells. To evaluate the anti-proliferative effect of GLD (chemical structure presented in Fig. 4A) on AML cell viability was assessed using the MTT assay. GLD treatment markedly inhibited the growth of HEL and K562 cells in a concentration- and time-dependent manner (Fig. 4C and D). The half-maximal inhibitory concentration (IC_{50}) for HEL cells was determined to be 3.039±0.692 μmol/l at 24 h, 0.808±0.166 μmol/l at 48 h and 0.385±0.011 μmol/l at 72 h. For K562 cells, the IC_{50} values were 5.165±0.768 μmol/l, 1.479±0.049 μmol/l and 0.388±0.010 μmol/l at 24, 48 and 72 h, respectively (Fig. 4B). The progressive leftward shift of the dose-response curves with prolonged exposure (Fig. 4C and D) visually represents a strong time-dependent effect, which is quantitatively corroborated by the marked decrease in IC_{50} values over time (Fig. 4B). Notably, HEL cells exhibited consistently lower IC_{50} values and left-shifted inhibition curves compared with K562 cells at both 24 and 48 h, indicating greater sensitivity to GLD. This differential sensitivity aligns with the distinct molecular background of the two cell lines; HEL cells harbor the activating JAK2 V617F mutation, which confers constitutive JAK-STAT pathway activation and may render them more susceptible to agents targeting this signaling axis. Furthermore, the IC_{50} of GLD against K562 cells at 48 h is similar to that reported for the classic chemotherapeutic agent cytarabine (~1.95 μmol/l in the same cell line) (18), indicating potent anti-proliferative activity of GLD *in vitro*. Morphological assessment of nuclear changes was performed using Hoechst 33258 staining. Compared with control cells, GLD-treated cells exhibited intensely stained, condensed nuclei, a morphological hallmark often associated with DNA damage and apoptosis (Fig. 4E).

GLD induces apoptosis in AML cell lines. To further investigate the effects of GLD on the survival of AML cell lines, flow cytometry was performed in the present study. AML cell lines were treated with GLD at concentrations of 0.25, 0.5 and 1 μmol/l for 48 h, followed by Annexin V-FITC/PI staining and flow cytometry analysis (Fig. 5A). Compared with the control group, the apoptosis rates in HEL and K562 cells treated with 0.25, 0.5 and 1 μmol/l GLD exhibited a progressive significant increase in association with the increasing concentrations of GLD (Fig. 5B and C).

GLD blocks AML cells in the G_2/M phase. To further investigate the effects of GLD on the AML cell cycle, the present study observed a progressive significant increase in the proportion of cells in the G_2/M phase with increasing concentrations of GLD. This finding indicated that GLD induces cell cycle arrest specifically at the G_2/M phase (Fig. 5D-F).

GLD exerts its anti-AML effects by targeting the JAK-STAT signaling pathway, leading to the induction of apoptosis and G_2/M phase arrest. To experimentally validate the mechanism predicted by computational analysis, the present study examined the effect of GLD on the JAK-STAT axis and its functional consequences. Western blotting analysis revealed that GLD treatment significantly inhibited the phosphorylation of JAK2

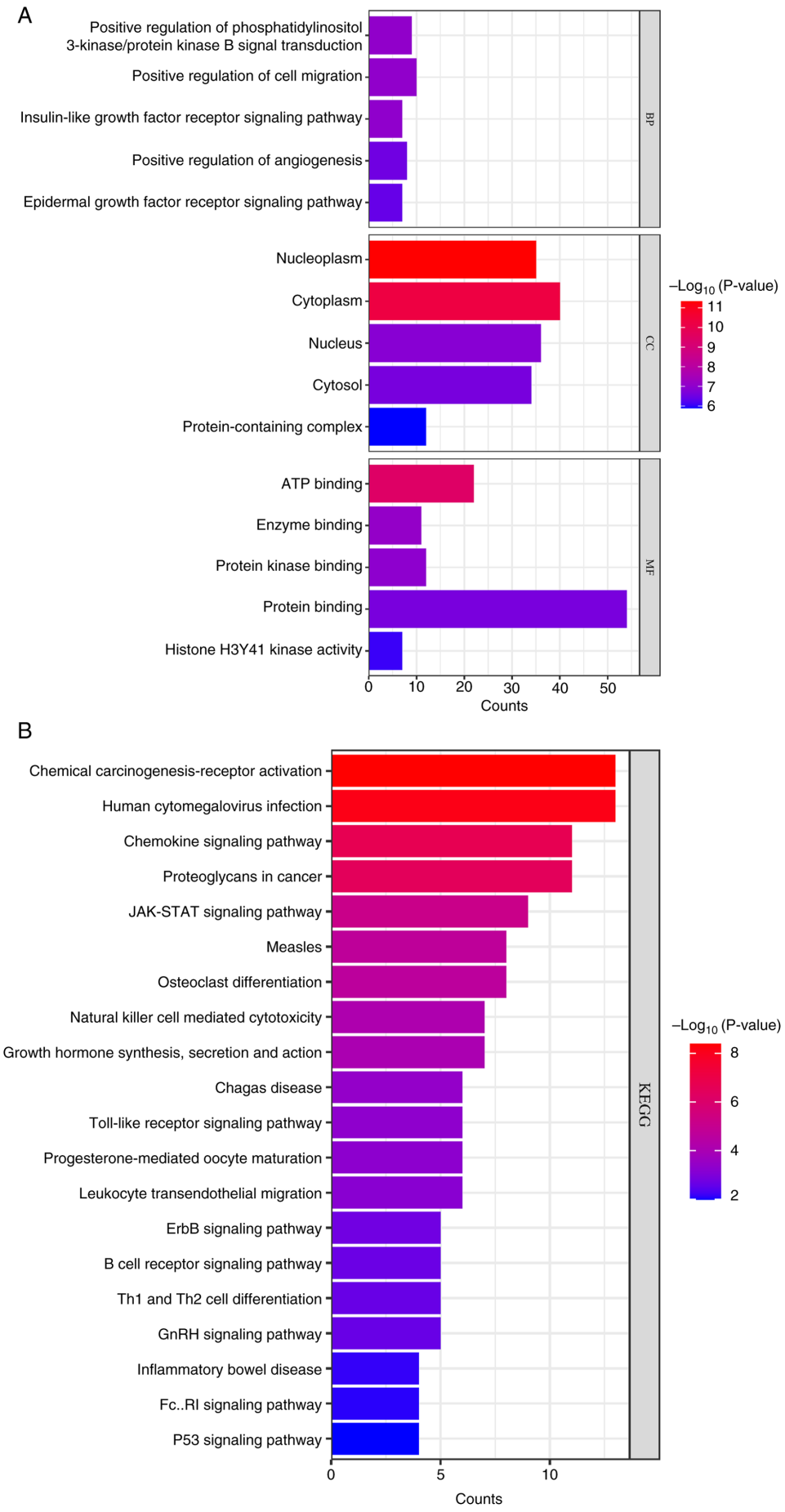

Figure 2. Enrichment analysis. (A) GO biological function analysis; (B) KEGG pathway enrichment analysis: Top 20 significantly enriched pathways [-log10 (P-value)]. GO, Gene Ontology; KEGG, Kyoto Encyclopedia of Genes and Genomes.

Table I. Annotation analysis of the top 20 KEGG signaling pathways.

Pathway	P-value	Count	Targets
Chemical carcinogenesis-receptor activation	$4.08x10^{-9}$	13	STAT1, STAT3, TLR4 and NFKB1
Human cytomegalovirus infection	$7.20x10^{-9}$	13	HSP90AB1, STAT3, PRKCA, PIK3R1, CYP3A4, mTOR, NFKB1, AR, KLF5, Bcl-6, RPS6KA1, MAPK1 and GRB2
Chemokine signaling pathway	$1.92x10^{-7}$	11	ZAP70, PTK2B, MAPK1, PTPN11, GRB2, PRKCA and PIK3R1
Proteoglycans in cancer	$3.22x10^{-7}$	11	CHUK, SERPINE1, MAPK1, PIK3R1, TLR4 and NFKB1
JAK-STAT signaling pathway	$6.87x10^{-6}$	9	MAPK1, GRB2, PRKCA, PIK3R1 and mTOR
Measles	$1.89x10^{-5}$	8	MAPK1, GRB2, PRKCA and PIK3R1
Osteoclast differentiation	$2.28x10^{-5}$	8	CHUK, CCNE1, STAT1, CDK4, STAT3, PIK3R1, TLR4 and NFKB1
Natural killer cell-mediated cytotoxicity	$7.10x10^{-5}$	7	CCR1, PDGFRA, CHUK, ITGB3, STAT3, PRKCA, PIK3R1, mTOR, NFKB1, CDK4, PTK2B, MAPK1 and GRB2
Growth hormone synthesis, secretion and action	$8.97x10^{-5}$	7	STAT1, STAT3, MAPK1, GRB2, PRKCA, PIK3R1 and mTOR
Chagas disease	$3.84x10^{-4}$	6	CCR1, ITK, CHUK, STAT1, STAT3, PRKCD, PTK2B, MAPK1, GRB2, PIK3R1 and NFKB1
Toll-like receptor signaling pathway	$4.99x10^{-4}$	6	CHUK, STAT1, ITGB3, MAPK1, GRB2, PIK3R1, MAP3K14 and NFKB1
Progesterone-mediated oocyte maturation	$5.43x10^{-4}$	6	CHUK, STAT1, MAPK1, PIK3R1, TLR4, NFKB1
Leukocyte transendothelial migration	$6.64x10^{-4}$	6	CHUK, MAPK1, GRB2, PIK3R1 and NFKB1
ErbB signaling pathway	$1.80x10^{-3}$	5	HSP90AB1, RPS6KA1, CDK1, MAPK1, PIK3R1 and CDC25C

Table I. Continued.

Pathway	P-value	Count	Targets
B cell receptor signaling pathway	$2.22x10^{-3}$	5	ITGB1, ITGB3, STAT3, MAPK1, PTPN11, GRB2, PRKCA, PIK3R1, HIF1A, TLR4 and mTOR
Th1 and Th2 cell differentiation	$2.40x10^{-3}$	5	ZAP70, CHUK, STAT1, MAPK1 and NFKB1
GnRH signaling pathway	$2.40x10^{-3}$	5	PRKCD, PTK2B, MAPK1, GRB2 and PRKCA
Inflammatory bowel disease	$7.45x10^{-3}$	4	PDGFRB, PDGFRA, STAT1, STAT3, PTPN11, GRB2, PIK3R1, PTPN2 and mTOR
FcεRI signaling pathway	$8.43x10^{-3}$	4	CCNE1, CDK4, SERPINE1 and CDK1
p53 signaling pathway	$1.06x10^{-2}$	4	ITGB1, ITK, PTK2B, PTPN11, PRKCA and PIK3R1

FcεRI, Fc ε receptor I; GnRH, gonadotropin-releasing hormone; Th1/2, T helper 1/2 cell; ErbB, erythroblastic leukemia viral oncogene homolog.

and its key downstream effector, STAT3, in AML cells in a dose-dependent manner, demonstrating an effective suppression of this pathway at the upstream level. This suppression elicited coordinated pro-apoptotic and cell cycle-disruptive responses. Specifically, GLD significantly downregulated the anti-apoptotic protein Bcl-2 and significantly upregulated the pro-apoptotic protein Bax, thereby shifting the cellular balance toward apoptosis. Concurrently, GLD significantly reduced the protein levels of cyclin B1 and its catalytic partner CDK1, the key driver complex for the G_2/M phase transition, which explains the observed cell cycle arrest (Fig. 6A-D). Collectively, these results outlined a coherent mechanistic pathway: GLD inhibits the JAK2-STAT3 signaling axis, which in turn orchestrates mitochondrial apoptosis and G_2/M phase cell cycle blockade in AML cells.

Discussion

AML is an aggressive hematological malignancy associated with a relapse rate of ~50% ≤1 year of achieving complete remission and therapeutic resistance, highlighting an urgent need for novel agents with distinct mechanisms of action (19). Natural products serve as a valuable source of such candidates due to their structural diversity and multi-target potential (20,21). Although diterpenoids such as GLA and GLB have demonstrated anticancer activities, the specific mechanism by which GLD exerts its effects against AML remains insufficiently explored, representing a key knowledge gap. The present study is the first to employ an integrated strategy combining network pharmacology, molecular docking and experimental validation to systematically elucidate the anti-AML mechanism of GLD, to the best of our knowledge. The core finding of the present study revealed that GLD exerts potent anti-leukemic effects primarily by inhibiting the JAK-STAT signaling pathway, thereby inducing mitochondrial apoptosis and G_2/M phase cell cycle arrest.

Network pharmacology analysis identified 55 potential overlapping targets between GLD and AML. Construction of a PPI network highlighted core targets including STAT3, STAT1, NFKB1, HSP90AB1, HIF1A and mTOR, suggesting that GLD may act through a multi-target, multi-pathway network. To functionally annotate these targets, GO and KEGG enrichment analyses were performed. GO analysis indicated extensive involvement in fundamental oncogenic processes, whereas KEGG analysis identified the 'JAK-STAT signaling pathway' as one of the most significantly enriched pathways. Notably, key target genes within this pathway, such as JAK2, STAT3 and Bcl-2, were specifically identified, providing precise hypotheses for subsequent molecular validation. Molecular docking further supported the structural feasibility of GLD binding to the core target STAT3. Due to the well-documented, pivotal role of the JAK-STAT signaling axis in AML pathogenesis (22-25), this pathway was prioritized for definitive experimental validation in the present study.

Based on these predictions, *in vitro* experiments confirmed that GLD effectively inhibits AML cell proliferation. Using HEL and K562 cells for mechanistic exploration, MTT assays demonstrated that GLD significantly and dose-dependently

Table II. Binding energy in molecular docking between glaucocalyxin D and core targets.

Target symbol	PDB ID	Binding energy, kcal/mol	Hydrogen bonds	Hydrophobic interactions	Salt bridges	π-stacking
PTPN11	Q06124	-7.7	LYS-2.22	THR-3.17	LYS-4.49 and LYS-5.40	LYS-4.49 and LYS-5.40
HSP90AB1	P08238	-7.1	ILE-2.06 and ILE-2.60	PHE-3.99, ILE-3.67 and GLN-3.03	LYS-5.26	LYS-5.26
MAPK1	P28482	-6.8	ALA-2.65, GLU-2.95 and GLU-2.35	ARG-3.98, ALA-3.66 and ALA-3.88	-	-
STAT1	P42224	-6.6	TYR-3.26, LYS-2.81 and ARG-2.46	-	LYS-3.74 and ARG-4.83	-
STAT3	P40763	-6.3	ARG-2.89	GLN-3.75, PRO-3.95 and ARG-3.82	-	-
HIF1A	Q309Z6	-5.8	-	-	-	-
GRB2	P62993	-5.6	-	-	-	-
TLR4	O00206	-5.3	-	-	-	-
mTOR	P42345	-4.9	-	-	-	-
NFKB1	P19838	-4.5	-	-	-	-

PDB ID, Protein Data Bank database identifier; LYS, lysine; THR, threonine; ARG, arginine; PRO, proline; GLN, glutamine; TYR, tyrosine; GLU, glutamic acid; ALA, alanine; ILE, isoleucine; PHE, phenylalanine; PTPN11, protein tyrosine phosphatase non-receptor type 11; HIF1A, hypoxia-inducible factor-1α; GRB2, growth factor receptor-bound protein 2; TLR4, toll-like receptor 4; HSP90AB1, heat shock protein 90 kDa α, class B, member 1; NFKB1, nuclear factor-κ B subunit 1.

suppressed proliferation in a time- and concentration-dependent manner. Notably, the anti-proliferative activity of GLD was similar to that of the clinical chemotherapeutic agent doxorubicin, employed as a positive control. This finding suggested the potential of GLD as a lead compound with efficacy rivaling current standard therapy. Furthermore, the multi-target profile inferred from network pharmacology may potentially offer a theoretical advantage in mitigating the drug resistance frequently encountered with single-target agents.

To validate the mechanistic basis of anti-AML action by GLD, the present study focused on key proteins within the JAK-STAT signaling pathway and cell-cycle regulators. The JAK-STAT pathway participates in diverse biological processes, including cell proliferation, differentiation, apoptosis and immune regulation (26,27). Dysregulation of this pathway is implicated in various cancer types, including hematological malignancies (for example, acute myeloid leukemia or myeloproliferative neoplasms) and solid tumors (for example, breast cancer or lung cancer), as well as autoimmune disorders such as rheumatoid arthritis, systemic lupus erythematosus and inflammatory bowel disease (24,25,28-31). Previous research indicated that constitutive STAT3 activation can suppress erythroid differentiation via upregulation of PU.1, thereby exacerbating erythroleukemia progression (32). By contrast, inhibitors of JAK2 or STAT3 phosphorylation can ameliorate anemia by restoring erythroid cell development (33). In the present study, western blotting analysis confirmed that GLD inhibited the phosphorylation of both JAK2 and STAT3 in a dose-dependent manner, as demonstrated by the reduced levels of phosphorylated p-JAK2 and p-STAT3 Apoptosis and cell-cycle arrest are two common indicators in antitumor research (34,35). Regarding apoptosis regulation, GLD significantly upregulated the pro-apoptotic protein Bax while downregulating the anti-apoptotic protein Bcl-2, representing a key molecular switch for initiating the mitochondrial-dependent intrinsic apoptotic pathway and mechanistically explaining GLD-induced apoptosis. In cell-cycle regulation, western blotting analysis demonstrated that GLD markedly downregulated the protein levels of cyclin B1 and its catalytic partner CDK1, core regulators of the G_2/M checkpoint. This suppression directly led to G_2/M phase arrest, which was fully consistent with flow cytometry results.

The present study findings underscored the therapeutic potential of GLD as a novel natural inhibitor of the JAK-STAT pathway, a key driver in AML. The implied multi-targeted potential may confer an advantage in modulating complex

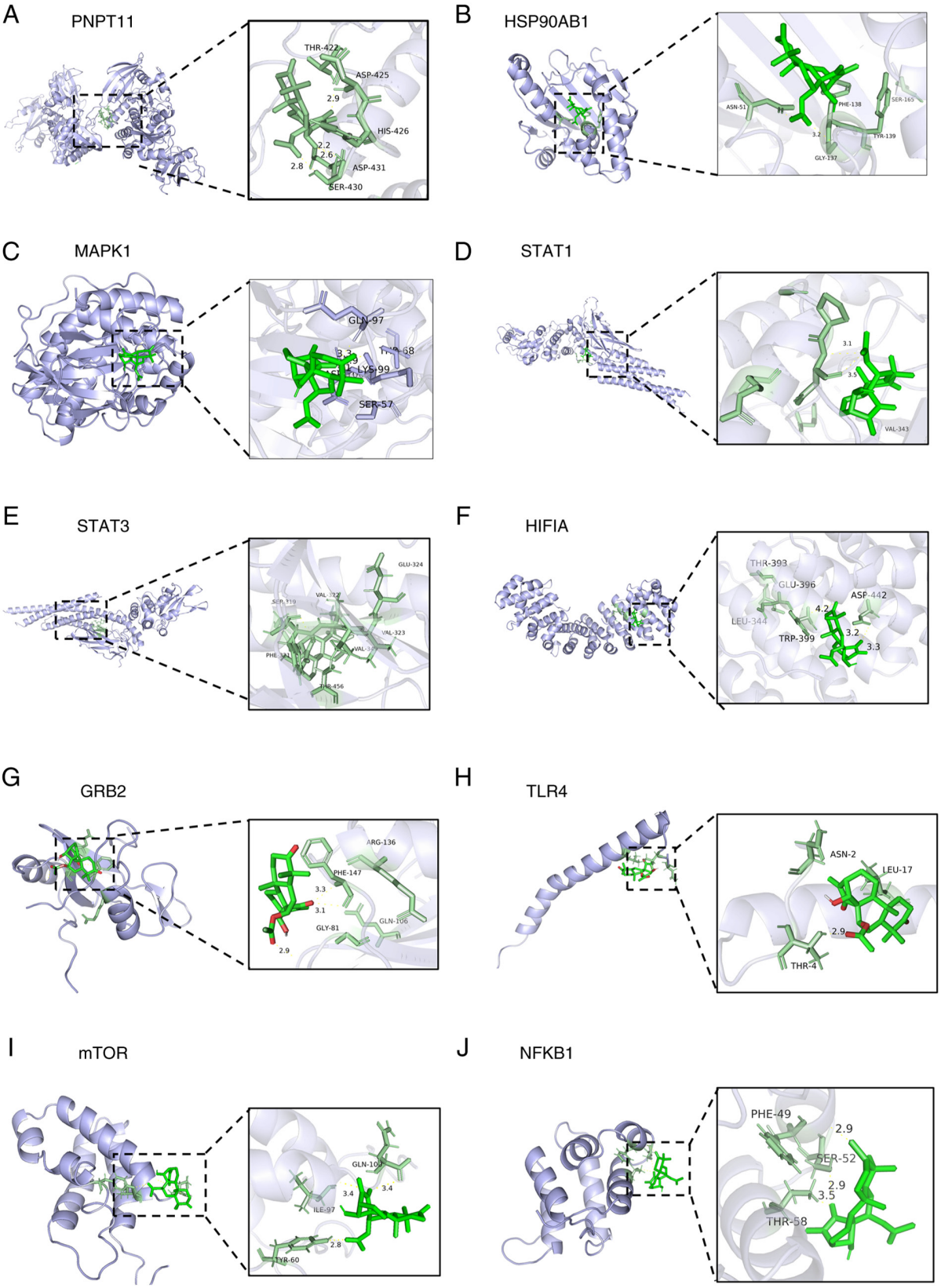

Figure 3. Docking results of glaucocalyxin D with 10 core target molecules. (A) PNPT11, (B) HSP90AB1, (C) MAPK1, (D) STAT1, (E) STAT3, (F) HIF1A, (G) GRB2, (H) TLR4, (I) mTOR, (J) NFKB1. Binding energies (kcal/mol) and detailed interactions (hydrogen bonds, hydrophobic interactions, salt bridges, π-stacking) for each target are presented in Table II. In the docking analysis, '-' indicates that no corresponding interaction was detected.

disease networks. However, certain limitations of the present study should be acknowledged. The validation was conducted primarily in established cell lines. Confirmation of the efficacy of GLD in primary patient-derived AML cells and relevant *in vivo* models is key to evaluating its translational potential and safety profile. Furthermore, to address potential

A

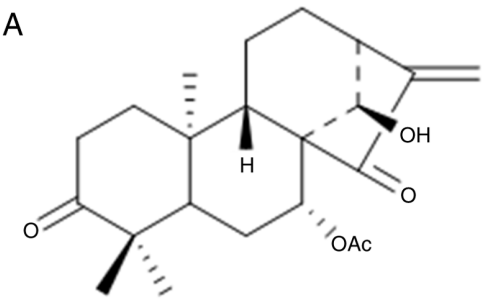

B

Compound	Time (h)	HEL	K562
GLD	24	3.039 ± 0.692	5.165 ± 0.768
	48	0.808 ± 0.166	1.479 ± 0.049
	72	0.385 ± 0.011	0.388 ± 0.010

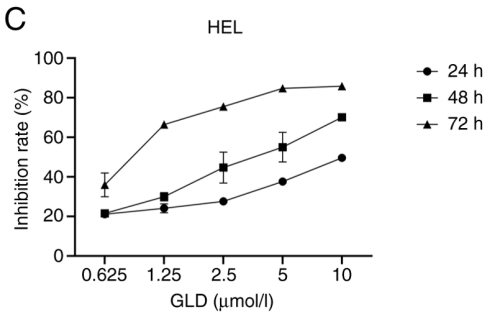

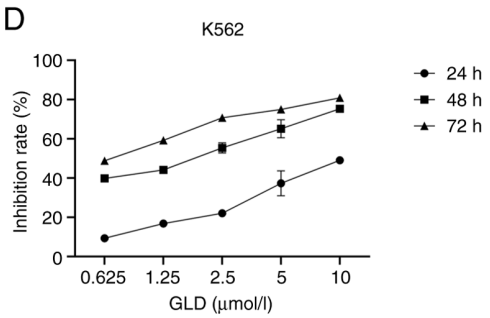

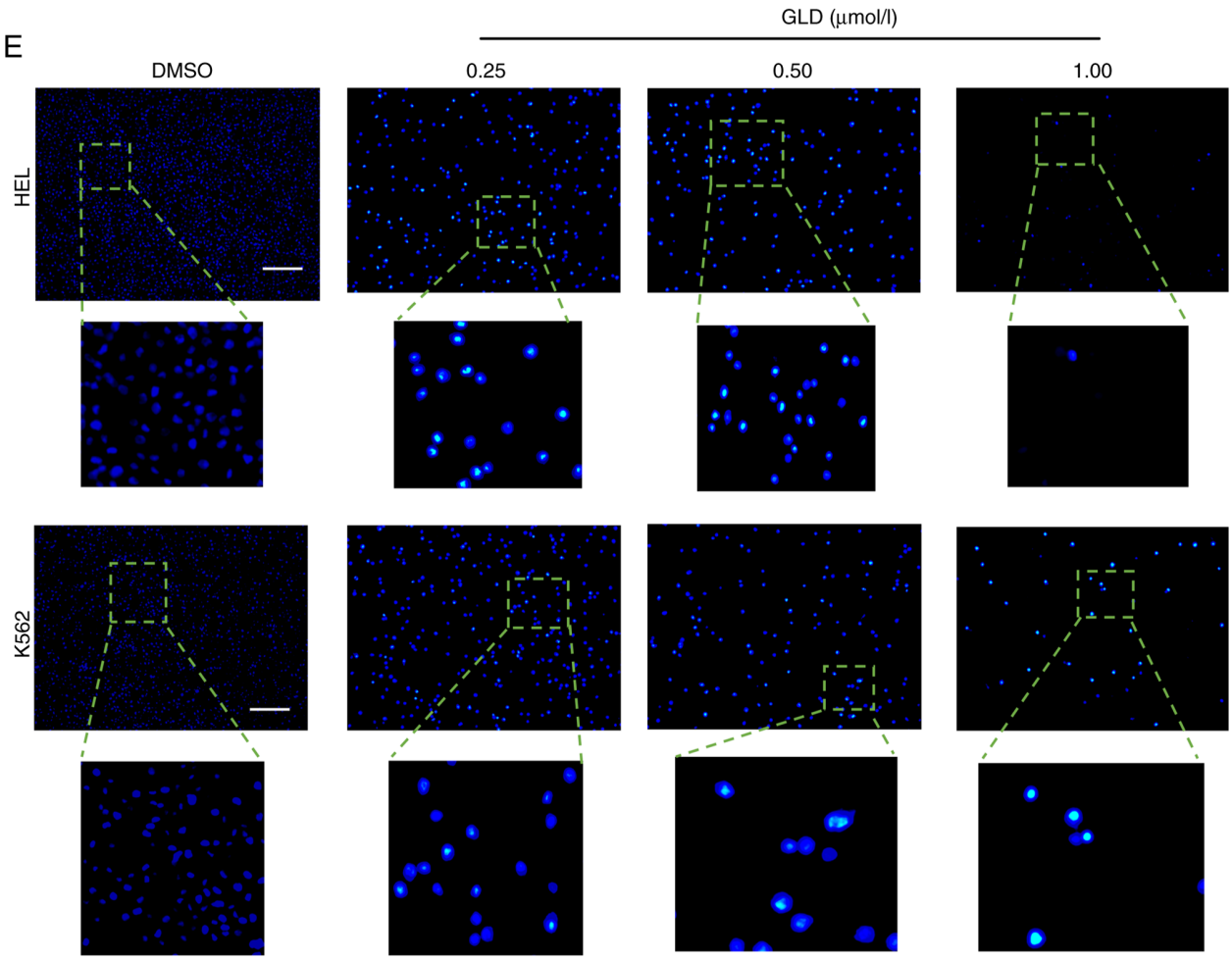

Figure 4. GLD inhibits the proliferation of AML cells. (A) Chemical structure of GLD. (B) IC50 values. (C) Inhibition rate in HEL cells. (D) Inhibition rate in K562 cells. (E) Hoechst 33258 staining with morphological changes observed under an inverted microscope (x100 magnification; scale bar, 100 μm). GLD, glaucocalyxin D; AML, acute myeloid leukemia.

pharmacokinetic challenges and enhance its therapeutic index, future research could explore advanced drug-delivery strategies. As highlighted by recent advances in nanocarrier technology, exemplified by antibody-functionalized lipid nanocarriers for targeted cancer therapy, encapsulating bioactive compounds such as GLD into optimized nano-formulations

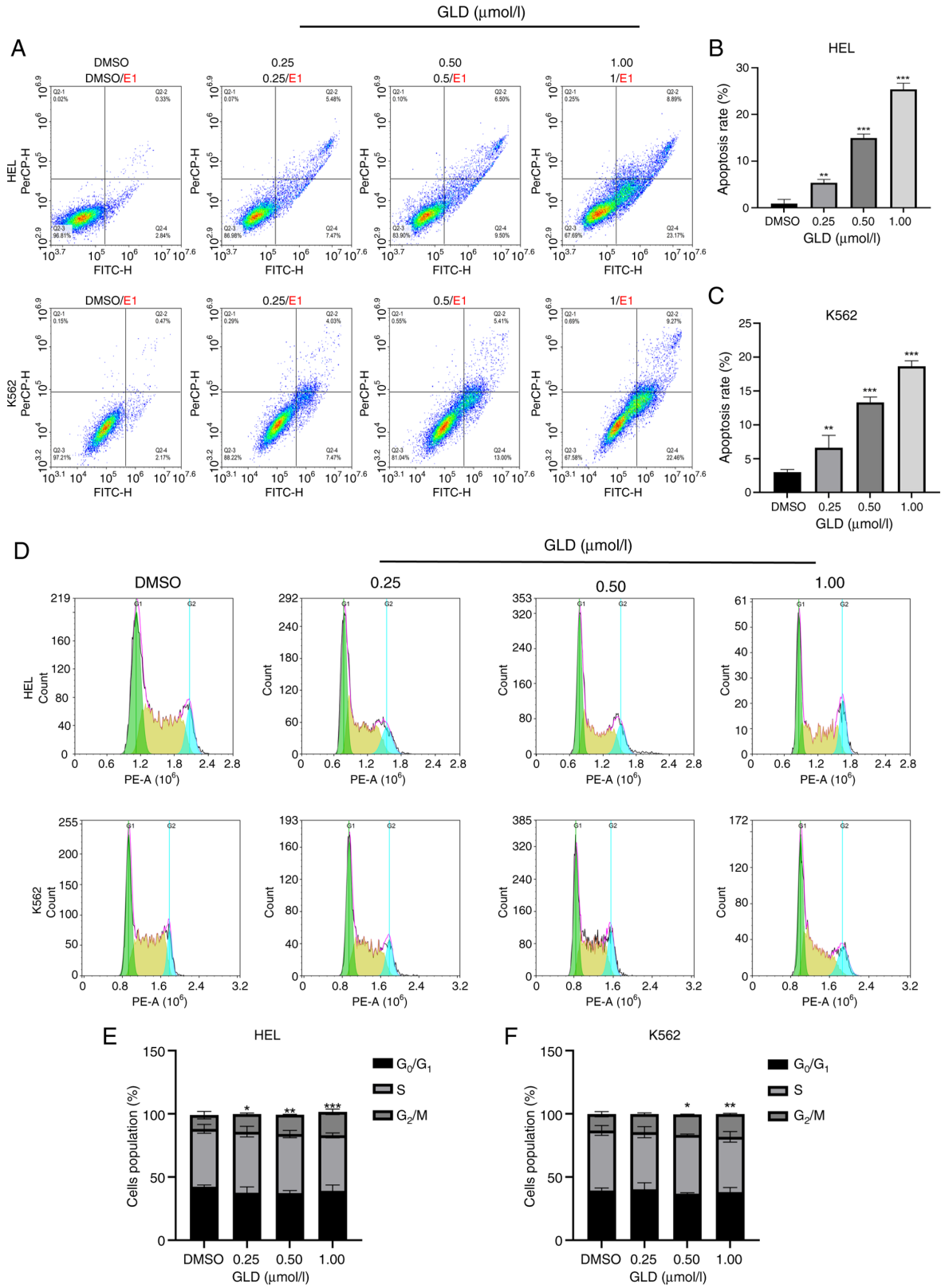

Figure 5. Flow cytometric analysis. (A) HEL and K562 cells treated with GLD at various concentrations (0.25, 0.5 and 1 μmol/l; DMSO as control) for 48 h. (B and C) Quantification of apoptotic cell percentage. (D) Analysis by flow cytometry of the effects of GLD on the cell cycle of HEL and K562 cells after 48 h (G_1 phase, green; S phase, yellow; G_2/M phase, blue). (E and F) Cell cycle statistics. Data are presented as mean ± SD (n=3). *P<0.05, **P<0.01 and ***P<0.001 compared with the control group. GLD, glaucocalyxin D.

could markedly improve its bioavailability, targeting specificity and reduce off-target toxicity, thereby facilitating clinical translation (36,37).

In conclusion, to the best of our knowledge, the present integrated study provides the first systematic evidence that GLD inhibits AML cell proliferation by suppressing the

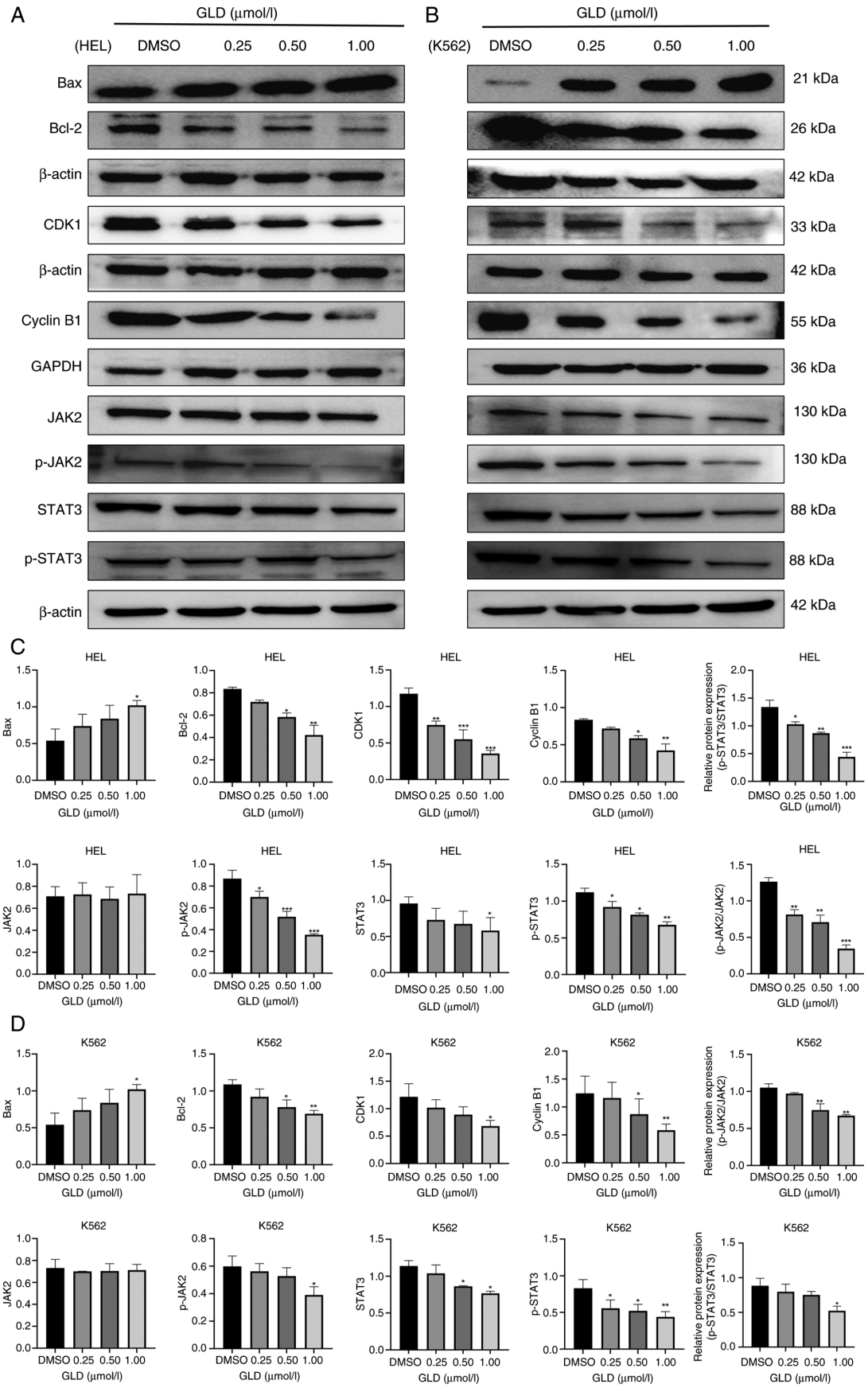

Figure 6. GLD exerts its anti-AML effects by targeting the JAK-STAT signaling pathway. (A) HEL cells were treated with the indicated concentrations of GLD (0, 0.25, 0.5 and 1 μmol/l) for 48 h. The protein expression levels of Bax, Bcl-2, CDK1, cyclin B1, JAK2, p-JAK2, STAT3 and p-STAT3 were detected by western blotting. β-actin and GAPDH were used as loading controls. (B) K562 cells were treated with GLD (0, 0.25, 0.5 and 1 μmol/l) for 48 h and the protein expression levels were detected as described in (A). (C) Quantification of the protein bands presented in (A) and (B). The relative protein expression levels were normalized to the loading controls, and p-JAK2 and p-STAT3 were further normalized to total JAK2 and STAT3, respectively. Data are presented as the mean ± SD (n=3). *P<0.05, **P<0.01 and ***P<0.001 vs. the control group. p, phosphorylated; AML, acute myeloid leukemia; GLD, glaucocalyxin D.

JAK-STAT pathway, which orchestrates downstream apoptotic and cell-cycle-disruptive events. These findings not only elucidate a coherent molecular mechanism for GLD but also potentially establishes GLD as a promising lead compound targeting the JAK-STAT axis for AML therapy in the future.

In summary, the present study systematically elucidated the mechanism by which GLD exerts anti-AML effects *in vitro*. GLD acts by inhibiting the JAK-STAT signaling pathway and coordinately regulating key downstream executioners of apoptosis and the cell cycle (Bax/Bcl-2 and cyclin B1/CDK1). These findings identify GLD as a multi-targeted natural compound that inhibits the JAK-STAT signaling pathway, supporting its potential as a lead molecule for developing therapeutic strategies against AML subtypes with aberrant JAK-STAT signaling. Future research should aim to overcome current limitations using *in vivo* validation and formulation optimization to advance its translation into preclinical development.

Acknowledgements

Not applicable.

Funding

The present study was supported by grants from the National Natural Science Foundation of China (grant no. 82460687), the Natural Science Foundation of China (grant no. 82460838), the Department of Science and Technology of Guizhou Province [grant no. QKZC(2024)YB068], the Science and Technology Foundation Project of Guizhou Provincial Health Commission (grant no. GZWJK2024-241), the Organization Department of Guizhou Provincial Committee [grant no. QKHPTRC-GCC(2022)034-2] and the Anshun City Science and Technology Plan Project [grant no. ASKSS(2024)01].

Availability of data and materials

The data generated in the present study may be requested from the corresponding author.

Authors' contributions

LC wrote the main manuscript and completed the main experiments under the supervision of CY and HL. LC and CY conceived and designed the study. HL contributed to the interpretation of data and critically revised the manuscript. WY isolated the compound and performed the structural characterization; WZ assisted in compound isolation. LC and CY confirm the authenticity of all the raw data. All authors reviewed and approved the final manuscript and agree to be accountable for all aspects of the work.

Ethics approval and consent to participate

Not applicable.

Patient consent for publication

Not applicable.

Competing interests

The authors declare that they have no competing interests.

References

1. Schratz KE and Armanios M: Cancer and myeloid clonal evolution in the short telomere syndromes. Curr Opin Genet Dev 60: 112-118, 2020.
2. Cai SF and Levine RL: Genetic and epigenetic determinants of AML pathogenesis. Semin Hematol 56: 84-89, 2019.
3. Weinberg OK, Sohani AR, Bhargava P and Nardi V: Diagnostic work-up of acute myeloid leukemia. Am J Hematol 92: 317-321, 2017.
4. Long L, Assaraf YG, Lei ZN, Peng H, Yang L, Chen ZS and Ren S: Genetic biomarkers of drug resistance: A compass of prognosis and targeted therapy in acute myeloid leukemia. Drug Resist Updat 52: 100703, 2020.
5. Yang GX, Ma GL, Li H, Huang T, Xiong J and Hu JF: Advanced natural products chemistry research in China between 2015 and 2017. Chin J Nat Med 16: 881-906, 2018.
6. Mansoori B, Mohammadi A, Amin Doustvandi M, Mohammadnejad F, Kamari F, Gjerstorff MF, Baradaran B and Hamblin MR: Photodynamic therapy for cancer: Role of natural products. Photodiagnosis Photodyn Ther 26: 395-404, 2019.
7. Gao C, Yu S and Liang Q: New research progress on Rabdosia japonica var. glaucocalyx. J Mudanjiang Med Univ 32: 54-56, 2011 (In Chinese).
8. Su Y, Cui J, Shi W, Wang X and Zhou Y: Research progress on Chinese herbal medicine isodon. Asia Pac Tradit Med 7: 155-161, 2011 (In Chinese).
9. Dong R, Gao H and Liu Z: Research progress on the biological activities of diterpenoids from isodon (lamiaceae). China Pharm 21: 651-653, 2010 (In Chinese).
10. Lin W, Xie J, Xu N, Huang L, Xu A, Li H, Li C, Gao Y, Watanabe M, Liu C and Huang P: Glaucocalyxin A induces G2/M cell cycle arrest and apoptosis through the PI3K/Akt pathway in human bladder cancer cells. Int J Biol Sci 14: 418-426, 2018.
11. Hou X, Xu G, Wang Z, Zhan X, Li H, Li R, Shi W, Wang C, Chen Y, Ai Y, *et al*: Glaucocalyxin A alleviates LPS-mediated septic shock and inflammation via inhibiting NLRP3 inflammasome activation. Int Immunopharmacol 81: 106271, 2020.
12. Gan P, Zhang L, Chen Y, Zhang Y, Zhang F, Zhou X, Zhang X, Gao B, Zhen X, Zhang J and Zheng LT: Anti-inflammatory effects of glaucocalyxin B in microglia cells. J Pharmacol Sci 128: 35-46, 2015.
13. Pan Y, Bai J, Shen F, Sun L, He Q and Su B: Glaucocalyxin B induces apoptosis and autophagy in human cervical cancer cells. Mol Med Rep 14: 1751-1755, 2016.
14. Wei MQ, Chen L, Zhang WQ, Sun M, Wang JJ, Zhan JP, Wang CL and Yan C: Chemical constituents from *Isodon suzhouensis* and their anti-tumor activity. Nat Prod Res Deve 37: 262-270+261, 2024 (In Chinese).
15. Zhao L, Zhang H, Li N, Chen J, Xu H, Wang Y and Liang Q: Network pharmacology, a promising approach to reveal the pharmacology mechanism of Chinese medicine formula. J Ethnopharmacol 309: 116306, 2023.
16. Yuan Z, Pan Y, Leng T, Chu Y, Zhang H, Ma J and Ma X: Progress and prospects of research ideas and methods in the network pharmacology of traditional Chinese medicine. J Pharm Pharm Sci 25: 218-226, 2022.
17. Dean PN and Jett JH: Mathematical analysis of DNA distributions derived from flow microfluorometry. J Cell Biol 60: 523-527, 1974.
18. Zhu XJ, Li YM, Gu JY, Guo M and Fei J: Enhanced Chemosensitivty of Leukemic Cells to Cytarabine by Targeted Suppression of miRNA-21. Life Sci Res 15: 317-322, 2011 (In Chinese).
19. Wang ES, Montesinos P, Foran J, Erba H, Rodríguez-Arbolí E, Fedorov K, Heiblig M, Heidel FH, Altman JK, Baer MR, *et al*: Ziftomenib in relapsed or refractory NPM1-mutated AML. J Clin Oncol 43: 3381-3390, 2025.
20. Atanasov AG, Waltenberger B, Pferschy-Wenzig EM, Linder T, Wawrosch C, Uhrin P, Temml V, Wang L, Schwaiger S, Heiss EH, *et al*: Discovery and resupply of pharmacologically active plant-derived natural products: A review. Biotechnol Adv 33: 1582-1614, 2015.
21. Aung TN, Qu Z, Kortschak RD and Adelson DL: Understanding the effectiveness of natural compound mixtures in cancer through their molecular mode of action. Int J Mol Sci 18: 656, 2017.

22. Hirose R, Miura T, Sha R, Shinkai Y, Tanaka-Kagawa T and Kumagai Y: A method for detecting covalent modification of sensor proteins associated with 1,4-naphthoquinone-induced activation of electrophilic signal transduction pathways. J Toxicol Sci 37: 891-898, 2012.
23. Furtek SL, Backos DS, Matheson CJ and Reigan P: Strategies and approaches of targeting STAT3 for cancer treatment. ACS Chem Biol 11: 308-318, 2016.
24. Fasouli ES and Katsantoni E: JAK-STAT in early hematopoiesis and leukemia. Front Cell Dev Biol 9: 669363, 2021.
25. How J, Garcia JS and Mullally A: Biology and therapeutic targeting of molecular mechanisms in MPNs. Blood 141: 1922-1933, 2023.
26. Jaśkiewicz A, Domoradzki T and Pająk B: Targeting the JAK2/STAT3 pathway-can we compare it to the two faces of the god janus? Int J Mol Sci 21: 8261, 2020.
27. Agashe RP, Lippman SM and Kurzrock R: JAK: Not just another kinase. Mol Cancer Ther 21: 1757-1764, 2022.
28. Qin JJ, Yan L, Zhang J and Zhang WD: STAT3 as a potential therapeutic target in triple negative breast cancer: A systematic review. J Exp Clin Cancer Res 38: 195, 2019.
29. Gao SP, Mark KG, Leslie K, Pao W, Motoi N, Gerald WL, Travis WD, Bornmann W, Veach D, Clarkson B and Bromberg JF: Mutations in the EGFR kinase domain mediate STAT3 activation via IL-6 production in human lung adenocarcinomas. J Clin Invest 117: 3846-3856, 2007.
30. Banerjee S, Biehl A, Gadina M, Hasni S and Schwartz DM: JAK-STAT signaling as a target for inflammatory and autoimmune diseases: Current and future prospects. Drugs 77: 521-546, 2017.
31. Salas A, Hernandez-Rocha C, Duijvestein M, Faubion W, McGovern D, Vermeire S, Vetrano S and Vande Casteele N: JAK-STAT pathway targeting for the treatment of inflammatory bowel disease. Nat Rev Gastroenterol Hepatol 17: 323-337, 2020.
32. Hegde S, Ni S, He S, Yoon D, Feng GS, Watowich SS, Paulson RF and Hankey PA: Stat3 promotes the development of erythroleukemia by inducing Pu.1 expression and inhibiting erythroid differentiation. Oncogene 28: 3349-3359, 2009.
33. Chen C, Lu M, Lin S and Qin W: The nuclear gene rpl18 regulates erythroid maturation via JAK2-STAT3 signaling in zebrafish model of Diamond-Blackfan anemia. Cell Death Dis 11: 135, 2020.
34. Fuchs Y: The therapeutic promise of apoptosis. Science 363: 1050-1051, 2019.
35. Talib WH: Melatonin and cancer hallmarks. Molecules 23: 518, 2018.
36. Nabih NW, Hassan HAFM, Preis E, Schaefer J, Babker A, Abbas AM, Amin MU, Bakowsky U and Fahmy SA: Antibody-functionalized lipid nanocarriers for RNA-based cancer gene therapy: Advances and challenges in targeted delivery. Nanoscale Adv 7: 5905-5931, 2025.
37. Wafik Nabih N, Nafie MS, Babker A, Hassan HAFM and Fahmy SA: Recent advances in nano vehicles encapsulating cinnamic acid and its derivatives as promising anticancer agents. RSC Adv 15: 20815-20847, 2025.